

High-energy magnon dispersion and multi-magnon continuum in the two-dimensional Heisenberg antiferromagnet

Anders W. Sandvik¹ and Rajiv R. P. Singh²

¹*Department of Physics, University of Illinois at Urbana-Champaign, 1110 West Green Street, Urbana, Illinois 61801*

²*Department of Physics, University of California, Davis, California 95616*

(October 30, 2018)

We use quantum Monte Carlo simulations and numerical analytic continuation to study high-energy spin excitations in the two-dimensional $S = 1/2$ Heisenberg antiferromagnet at low temperature. We present results for both the transverse (x) and longitudinal (z) dynamic spin structure factor $S_{x,z}(\mathbf{q}, \omega)$ at $\mathbf{q} = (\pi, 0)$ and $(\pi/2, \pi/2)$. Linear spin-wave theory predicts no dispersion on the line connecting these momenta. Our calculations show that in fact the magnon energy at $(\pi, 0)$ is 10% lower than at $(\pi/2, \pi/2)$. We also discuss the transverse and longitudinal multi-magnon continua and their relevance to neutron scattering experiments.

PACS: 75.40.Gb, 75.40.Mg, 75.10.Jm, 75.30.Ds

It is now well established that the spin-wave theory of the two-dimensional Heisenberg model [1] correctly describes the low-energy dynamics of layered antiferromagnets such as La_2CuO_4 [2,3]. Several methods have been used to calculate the quantum renormalization factor Z of the spin wave velocity, $c = Zc_0$, with the result $Z \approx 1.18$ for $S = 1/2$ [4–8]. Early neutron scattering experiments were consistent with this renormalization over the entire Brillouin zone [9]. However, recently more accurate measurements have shown clear deviations at high energies in La_2CuO_4 [10] and other materials [11]. In particular, spin-wave theory predicts no dispersion on the magnetic zone boundary, i.e., along the line of momenta $\mathbf{q} = (\pi - x, x)$, whereas the experimental data show a significant variation in the excitation energy. This could be caused by interactions other than the nearest-neighbor super-exchange J normally used to model the materials [10,12]. The deviations could also be at least partially due to a failure of low-order spin-wave theory to account for the high-energy dynamics of the Heisenberg model. A series expansion calculation [13] indeed indicates a momentum dependent renormalization factor, with the magnon energy at $\mathbf{q} = (\pi, 0)$ approximately 7% lower than at $(\pi/2, \pi/2)$. This, however, is opposite to the trend found experimentally for La_2CuO_4 [10].

Another important issue, that has not yet been confronted experimentally, is the multi-magnon continuum expected to be present in the dynamic structure factor $S(\mathbf{q}, \omega)$ above the single-magnon mode. The neutron scattering cross-section has been analyzed assuming only a delta-function representing the spin waves with dispersion $\omega_{\mathbf{q}}$ [2,9–11]. The resolution of present experiments is not sufficient for detecting the presence of additional spectral weight, much less to determine its distribution. Theoretical calculations have so far also not been successful in accurately determining the full dynamic structure factor. In order to provide guidance for improved fitting procedures it is imperative to obtain quantitative estimates of the multi-magnon spectral features, in particu-

lar considering that experiments may soon become sufficiently accurate for detecting the continuum. Within spin-wave theory, correctly accounting for the interactions that give rise to the continuum is extremely complicated and has led to contradictory results [6,14,15]. Numerical calculations of $S(\mathbf{q}, \omega)$ are challenging because large lattices have to be used to converge to the thermodynamic limit, and the extraction of real-time dynamics from quantum Monte Carlo (QMC) data is difficult. Such calculations have therefore so far only given limited insights [16,17]. The series work [13] suggests a significant continuum but gives no information on its shape.

Here we address the issues of high-energy magnon dispersion and multi-magnon continuum using QMC calculations in a way that explicitly separates the transverse and longitudinal components of the dynamic structure factor. This allows us to more accurately determine both the magnon energy and the continuum part of the spectrum. We consider the Heisenberg model on a square lattice, defined in standard notation by the Hamiltonian

$$H = J \sum_{\langle i,j \rangle} \mathbf{S}_i \cdot \mathbf{S}_j. \quad (1)$$

The coupling $J \approx 1500$ K in typical planar cuprates. On an infinite lattice the spin-rotational symmetry of this model is spontaneously broken at $T = 0$ and long-range order develops along an axis that we take as the z -direction. The two-point correlations then have different longitudinal (z) and transverse (x, y) components. In a finite system the symmetry is not broken and all correlation functions are equal to the same rotational average. We want to access separately the transverse dynamic structure factor, which contains the single-magnon mode as well as a continuum, and the longitudinal component comprising only a multi-magnon continuum. To this end, we explicitly break the symmetry by applying a staggered magnetic field;

$$H \rightarrow H - h \sum_i (-1)^{x_i+y_i} S_i^z. \quad (2)$$

We adjust the field strength h so that the induced staggered magnetization equals the known value in the thermodynamic limit; $m = |\langle S_i^z \rangle| = 0.307$ [18,19,5–8]. In the limit of large system sizes $h \rightarrow 0$ (at $T = 0$) and the correlation functions become equal to their values in a system with spontaneously broken symmetry.

In real layered cuprates there is a small inter-layer coupling and some degree of anisotropy, resulting in a finite- T transition to an ordered state, in La_2CuO_4 at $T_N \approx 300$ K. We here consider a low temperature, $\beta = J/T = 32$, corresponding to approximately 50 K, where the staggered magnetization in real materials is very close to the saturated $T = 0$ value. Our staggered field h can then also be viewed as a mean-field treatment of the inter-layer coupling [20].

Working with lattices with $N = L \times L$ spins and periodic boundary conditions, we have used the stochastic series expansion method [21] to calculate the imaginary-time dependent spin-spin correlation function

$$G_\alpha(\mathbf{q}, \tau) = \langle S^\alpha(-\mathbf{q}, \tau) S^\alpha(\mathbf{q}, 0) \rangle, \quad (3)$$

where $\alpha = x, z$ and

$$S^a(\mathbf{q}, \tau) = \frac{1}{\sqrt{N}} \sum_i e^{-\mathbf{q} \cdot \mathbf{r}_i} e^{-\tau H} S_i^a e^{\tau H}. \quad (4)$$

The correlation function is related to the dynamic structure factor according to

$$G_\alpha(\mathbf{q}, \tau) = \frac{1}{\pi} \int_{-\infty}^{\infty} d\omega S_\alpha(\mathbf{q}, \omega) e^{-\tau\omega}, \quad (5)$$

which in principle can be inverted to yield the real-frequency dynamics from the correlation function computed in the simulations. With simulation data affected by statistical fluctuations there are well known difficulties in carrying out this analytic continuation in practice, and one can only expect limited frequency resolution using, e.g., the maximum entropy method [22]. Here we will instead assume reasonable functional forms for the transverse (x) and longitudinal (z) dynamic structure factors, with parameters that are adjusted to satisfy the equality (5). With the QMC method used, derivatives of $G_\alpha(\mathbf{q}, \tau)$ can also be directly calculated [23] and impose additional constraints on $S_\alpha(\mathbf{q}, \omega)$; from Eq. (5)

$$G_\alpha^{(n)}(\mathbf{q}, \tau) = \frac{(-1)^n}{\pi} \int_{-\infty}^{\infty} d\omega S_\alpha(\mathbf{q}, \omega) \omega^n e^{-\tau\omega}. \quad (6)$$

We use the first ($n = 1$) and ($n = 2$) second derivatives, which at $\tau = 0$ correspond to the first two frequency moments of the spectrum. We also use the sum rule

$$\chi_\alpha(\mathbf{q}) = \frac{2}{\pi} \int_{-\infty}^{\infty} \frac{d\omega}{\omega} S_\alpha(\mathbf{q}, \omega), \quad (7)$$

where $\chi_\alpha(\mathbf{q})$ is the static susceptibility

$$\chi_\alpha(\mathbf{q}) = \int_0^\beta d\tau G_\alpha(\mathbf{q}, \tau). \quad (8)$$

The spectrum also obeys the bosonic relation $S_\alpha(\mathbf{q}, -\omega) = e^{-\beta\omega} S_\alpha(\mathbf{q}, \omega)$.

For the model forms of the transverse and longitudinal structure factors we take simple functions that reflect the expected gross spectral features. The transverse component should include a delta-function at an energy $\omega_{\mathbf{q}}$, representing the magnon, and a continuum that does not extend below $\omega_{\mathbf{q}}$ (temperature broadening of the high-energy magnons should be insignificant at $\beta = 32$). The longitudinal component is entirely in the continuum and can also not extend below $\omega_{\mathbf{q}}$. Both continua must decay to zero rapidly as $\omega \rightarrow \infty$, to ensure convergence of all frequency moments. We use

$$S_x(\mathbf{q}, \omega) = A_1(\mathbf{q}) \delta(\omega - \omega_{\mathbf{q}}) + A_2(\mathbf{q}) f_x(\mathbf{q}, \omega), \quad (9)$$

$$S_z(\mathbf{q}, \omega) = B(\mathbf{q}) f_z(\mathbf{q}, \omega), \quad (10)$$

where the continua $f_{x,z}(\mathbf{q}, \omega)$ are given by

$$f_x(\mathbf{q}, \omega) = r_x e^{-(\omega - \nu)^2 / 2\sigma^2}, \quad (0 \text{ for } \omega < \omega_{\mathbf{q}}), \quad (11)$$

$$f_z(\mathbf{q}, \omega) = r_z (\omega - \omega_{\mathbf{q}})^p e^{-a(\omega - \omega_{\mathbf{q}})^b}, \quad (0 \text{ for } \omega < \omega_{\mathbf{q}}), \quad (12)$$

where r_x and r_z are factors normalizing the frequency integrals to unity. For clarity, we have suppressed the dependence of the parameters ν, σ, p, a , and b on \mathbf{q} . The static structure factors (the integrated spectral weights) are given by

$$S_x(\mathbf{q}) = \langle S^x(-\mathbf{q}) S^x(\mathbf{q}) \rangle = A_1(\mathbf{q}) + A_2(\mathbf{q}), \quad (13)$$

$$S_z(\mathbf{q}) = \langle S^z(-\mathbf{q}) S^z(\mathbf{q}) \rangle = B(\mathbf{q}). \quad (14)$$

In scattering experiments with unpolarized neutrons, a rotational average of the transverse and longitudinal dynamic structure factors is measured. The rotationally averaged static structure factor $S(\mathbf{q}) = 2S_x(\mathbf{q}) + S_z(\mathbf{q}) = 2A_1 + 2A_2 + B$.

The values we find for the “self-consistent” staggered field (demanding $m = 0.3070$ to an accuracy of better than 0.00005) are $h/J = 0.10652$ for $L = 4$, 0.022575 for $L = 8$, 0.005450 for $L = 16$, and 0.001615 for $L = 32$. With the QMC algorithm [21] implemented in the z -basis, and with the field also in the z -direction, the longitudinal correlations can be easily calculated. In order to compute the transverse correlations it is more efficient to apply the field in the x -direction, so that the measurements can be carried out with diagonal operators [24]. Hence, we perform two independent simulations for each lattice size.

Fig. 1 shows our results for the ratio of the longitudinal and transverse spectral weights versus the momentum, along a standard path in the Brillouin zone. At $\mathbf{q} = (\pi, \pi)$ the ratio diverges (in the thermodynamic limit), reflecting the divergence of $S_z(\pi, \pi)$ due to the long-range order.

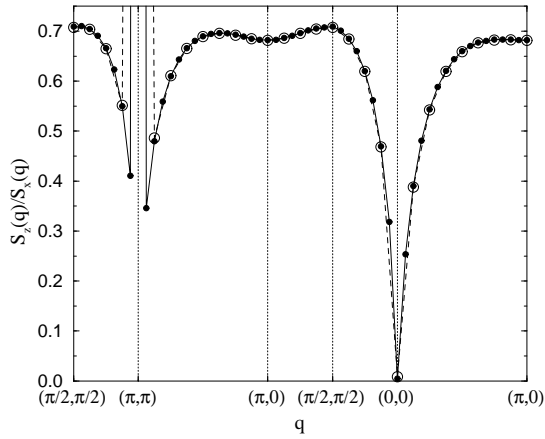


FIG. 1. Ratio of the longitudinal and transverse static structure factors (integrated spectral weights) along a path in the Brillouin zone. Open circles are for $L = 16$ and solid ones for $L = 32$.

For $\mathbf{q} \rightarrow (0, 0)$ and $\mathbf{q} \rightarrow (\pi, \pi)$ it approaches zero and hence the magnon completely exhausts the total spectral weight in these limits (other treatments have shown that the magnon exhausts the low-energy transverse spectral weight [25]). The ratio is the largest at $\mathbf{q} = (\pi/2, \pi/2)$ where it is above 0.7 — it is between 0.6 and 0.7 over much of the Brillouin zone. Hence, in unpolarized neutron scattering experiments, 30 – 35% of the cross-section at the zone boundary is due to the longitudinal continuum.

Next we study the full dynamic structure factor, focusing on the zone-boundary momenta $\mathbf{q} = (\pi, 0)$ and $(\pi/2, \pi/2)$. The analytic continuation using fits to the functions (9) and (10) was carried out using QMC imaginary-time data with a spacing $\Delta\tau = 0.5$ up to $\tau = 4$ (the data become too noisy for higher τ). For $L = 4$, we have compared with exact diagonalization results and find that the magnon energy is very accurately reproduced (better than 0.5%) but the weight in the magnon is underestimated by about 5% because the form of the continuum, Eq. (11), is not appropriate for a very small system where only a small number of significant delta-functions represent the continuum. Our results for larger systems should have smaller systematic errors.

Fig. 2 shows the size dependence of the magnon weight and energy (the scatter of the data gives an indication of the statistical errors). The $L = 4$ data is from exact diagonalization; in this case the two momenta are degenerate due to equivalence of this lattice and a 2^4 hyper-cube. Rough extrapolations in $1/L$ give the infinite-size energy $\omega_{\mathbf{q}}/J \approx 2.15$ for $\mathbf{q} = (\pi, 0)$ and 2.39 for $(\pi/2, \pi/2)$. The relative weight of the magnon in $S_x(\mathbf{q}, \omega)$ is $\approx 60\%$ at $(\pi, 0)$ and 85% at $(\pi/2, \pi/2)$. Within linear spin-wave theory, including the quantum-renormalization $Z = 1.18$, the energy $\omega_{\mathbf{q}}/J = 2.36$ for both momenta. Hence, the results show that the interactions neglected in spin-wave theory have strong effects at $\mathbf{q} = (\pi, 0)$, lowering the energy by almost 10% and transferring $\approx 40\%$ of the

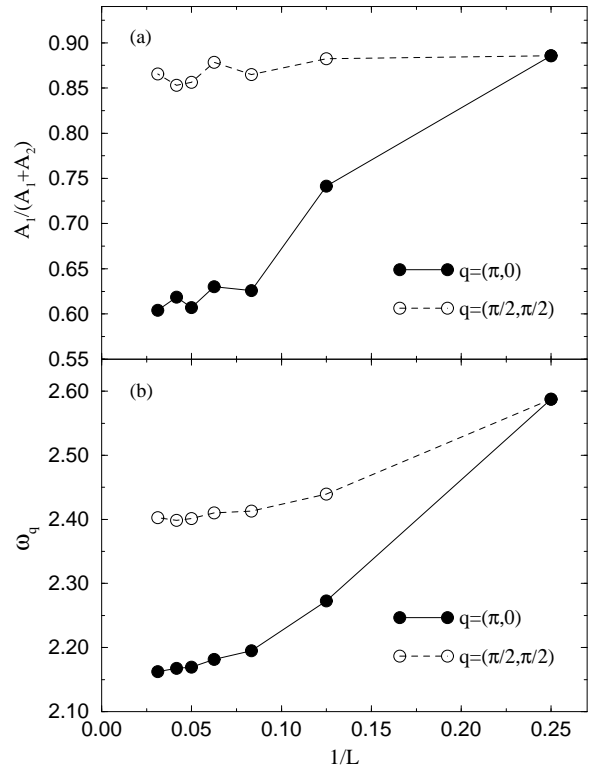


FIG. 2. Properties of the single-magnon part of the transverse dynamic structure factor vs inverse system size ($L = 4, 8, 12, 16, 20, 24$, and 32). (a) single-magnon fraction of the weight, (b) magnon energy.

magnon weight into the continuum. At $(\pi/2, \pi/2)$ the excitation energy is instead slightly increased by the interactions and a much smaller fraction of the weight is in the continuum.

Fig. 3 shows the magnon as well as the transverse and longitudinal continua for $L = 32$. The rotationally averaged structure factor measured in neutron scattering experiments with unpolarized neutrons is also shown. The exponent p in the longitudinal continuum, Eq. (12), is small and positive, $p \lesssim 0.05$, giving a spectral weight concentrated close to the magnon. The longitudinal continuum is significantly narrower at $(\pi/2, \pi/2)$ than at $(\pi, 0)$. For both momenta, the transverse continuum is broad and centered further above the magnon. All these spectral features are consistently present for system sizes $L \geq 8$. As seen in the insets of Fig. 3, for $L = 32$ only $\approx 45\%$ of the rotationally averaged spectral weight is in the magnon mode at $(\pi, 0)$, increasing to $\approx 65\%$ at $(\pi/2, \pi/2)$. The magnon weight decreases only slightly for even larger systems, as can be inferred from Fig. 2.

In previous work using QMC and analytic continuation [16,17], the magnon energy was extracted as the first moment of the rotationally averaged relaxation function, $F(\mathbf{q}, \omega) \sim S(\mathbf{q}, \omega)/\omega$. Using this procedure, we find the moment 2.53 at $(\pi, 0)$ and 2.58 at $(\pi/2, \pi/2)$, i.e., both significantly above the actual magnon energies (the first

moment of $S(\mathbf{q}, \omega)$ is higher yet; approximately 2.66 for both momenta). This is clearly due to the large spectral weight in the continuum. There is potentially a similar problem in the analysis of neutron scattering data. Since the present-day energy resolution is such that a non-negligible part of the continuum that we have found here would be included in an experimental fit to a single resolution-broadened peak, the extracted magnon energy may be too high. This effect would be particularly important at and close to $\mathbf{q} = (\pi, 0)$, where our results show that less than 50% of the total weight is in the magnon peak and the continuum is relatively broad.

Experimental results do appear to show the presence of some weight consistent with a continuum above the resolution-broadened magnon peak [10], but the statistics is not sufficient for extracting its size and shape. Our calculations should be useful for analyzing future experiments with higher resolution. Such experiments will be very important for determining the significance of other interactions in the antiferromagnetic cuprates beyond the nearest-neighbor exchange J . The significant effects of magnon interactions that we have found at $\mathbf{q} = (\pi, 0)$ may also have important consequences for the broadening of the Raman spectrum [15] and the momentum space anisotropy of the photoemission spectrum [26].

We would like to thank G. Aeppli, L. Balents, G. Sawatzky, and D. Scalapino for stimulating discussions. This research was supported by the NSF under grants No. DMR-97-12765 and DMR-99-86948. The work was started at the Institute of Theoretical Physics at UC Santa Barbara, under support of NSF grant No. PHY-94-07194. Most of the numerical calculations were carried out on the SGI Origin2000 system the NCSA.

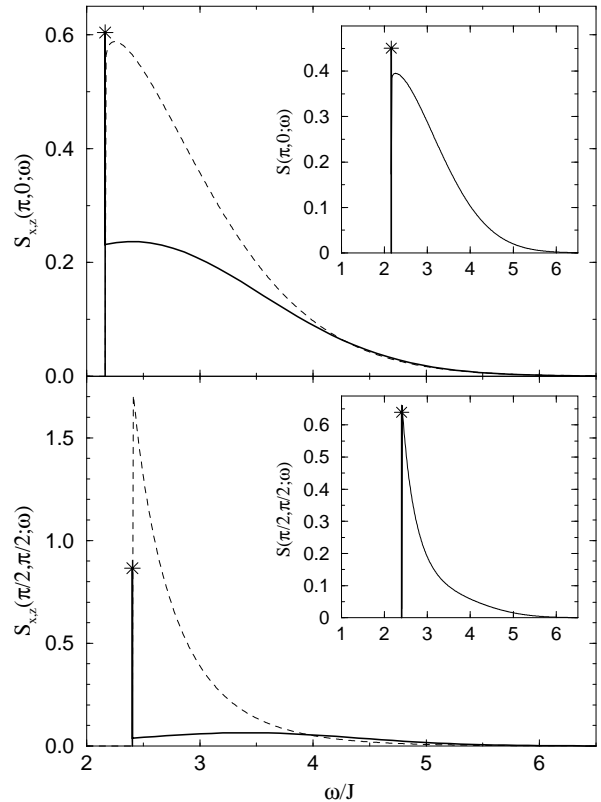


FIG. 3. The transverse (solid curves) and longitudinal (dashed curves) dynamic structure factor at $\mathbf{q} = (\pi, 0)$ (upper panel) and $(\pi/2, \pi/2)$ (lower panel). $S_x(\mathbf{q}, \omega)$ and $S_z(\mathbf{q}, \omega)$ are normalized to 1 and $S_z(\mathbf{q})/S_x(\mathbf{q})$ [see Fig. 1], respectively. The delta-function piece of $S_x(\mathbf{q}, \omega)$ is represented by a vertical line with height (indicated by a star) equal to its relative weight $A_1(\mathbf{q})$. The insets show the rotationally averaged spectra, $S(\mathbf{q}, \omega) = 2S_x(\mathbf{q}, \omega) + S_z(\mathbf{q}, \omega)$.

-
- [1] P. W. Anderson, Phys. Rev. **86**, 694 (1952).
[2] D. Vaknin *et al.*, Phys. Rev. Lett. **58**, 2802 (1987); G. Shirane *et al.*, *ibid.* **59**, 1613 (1987); G. Aeppli *et al.*, *ibid.* **62**, 2052 (1989).
[3] S. Chakravarty, B. I. Halperin, and D. R. Nelson, Phys. Rev. Lett. **60**, 1057 (1988); Phys. Rev. B **39**, 2344 (1989).
[4] T. Oguchi, Phys. Rev. **117**, 117 (1960).
[5] R. R. P. Singh, Phys. Rev. B **39**, 9760 (1989).
[6] C. J. Hamer, Z. Weihong, and P. Arndt, Phys. Rev. B **46**, 6276 (1992); J. Igarashi, Phys. Rev. B **46**, 10763 (1992); C. M. Canali and M. Wallin, Phys. Rev. B **48**, 3264 (1993).
[7] U.-J. Wiese and H.-P. Ying, Z. Phys. B **93**, 147 (1994); B. B. Beard and U.-J. Wiese, Phys. Rev. Lett. **77**, 5130 (1996).
[8] A. W. Sandvik, Phys. Rev. B **56**, 11678 (1997).
[9] S. Hayden *et al.*, Phys. Rev. Lett. **67**, 3622 (1991).
[10] R. Coldea *et al.* (unpublished).
[11] Y. J. Kim *et al.* Phys. Rev. Lett. **83**, 852 (1999); H. M. Rønnow *et al.* (unpublished).
[12] D. K. Morr, Phys. Rev. B **58**, R587 (1998).
[13] R. R. P. Singh and M. P. Gelfand, Phys. Rev. B **52**, 15695 (1995).
[14] J. Igarashi and A. Watabe, Phys. Rev. B **43**, 13456 (1991).
[15] C. M. Canali and S. M. Girvin, Phys. Rev. B **45**, 7127 (1992).
[16] M. S. Makivic and M. Jarrell, Phys. Rev. Lett. **68**, 1770 (1992).
[17] O. F. Syljuåsen and H. M. Rønnow, cond-mat/0003350.
[18] J. Oitmaa and D. D. Betts, Can. J. Phys. **56**, 897 (1978).
[19] J. D. Reger and A. P. Young, Phys. Rev. B **37**, 5978 (1988).
[20] D. J. Scalapino, Y. Imry, and P. Pincus, Phys. Rev. B **11**, 2042 (1975).
[21] A. W. Sandvik, Phys. Rev. B **59**, R14157 (1999).
[22] M. Jarrell and J. E. Gubernatis, Phys. Rep. **269**, 133 (1996).
[23] A. W. Sandvik, S. Capponi, D. Poilblanc, and E. Dagotto, Phys. Rev. B **57**, 8478 (1998).
[24] P. Henelius, A. W. Sandvik, and S. M. Girvin, Phys. Rev. B **61**, 364 (2000).
[25] S. Stringari, Phys. Rev. B **49**, 6710 (1994).
[26] B. O. Wells *et al.*, Phys. Rev. Lett. **74**, 964 (1995); C. Kim *et al.*, *ibid.*, **80**, 4245 (1998).